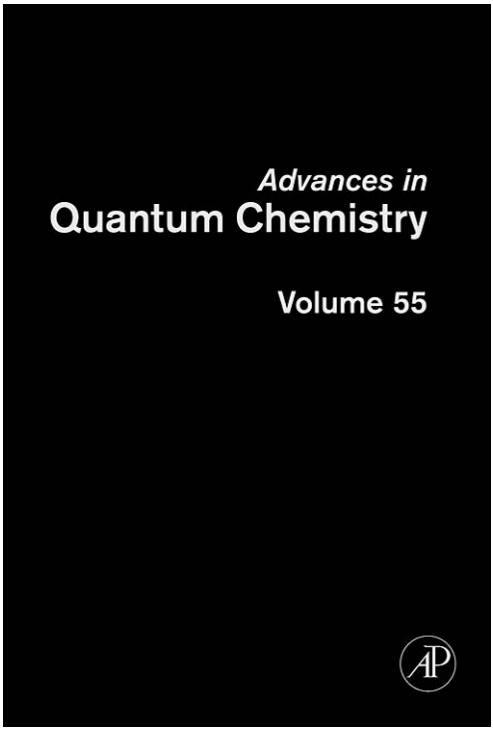

João Brandão, Carolina M.A. Rio and Wenli Wang, An Important Well Studied Atmospheric Reaction, O (^1D) + H_2. In: M.E. Goodsite and M.S. Johnson, editors, Advances in Quantum Chemistry, vol. 55. Amsterdam: Elsevier, 2008, p. 21.
ISBN: 978-0-12-374335-0

Elsevier Inc.

CHAPTER 3

An Important Well Studied Atmospheric Reaction, O (^1D) + H_2

João Brandão*, **Carolina M.A. Rio*** and **Wenli Wang***

Contents

Abstract

Among the chemical reactions in atmosphere, the reaction of an excited oxygen atom, O (^1D), with ground state molecular hydrogen, H_2 ($X\,^1\Sigma_g^+$), has been one of the most studied both experimentally and theoretically. To describe this reaction, various potential energy surfaces have been calibrated and their dynamics has been studied using quantum mechanical and quasiclassical trajectory methods. The theoretical results have shown to be in good agreement with experiment. The main uncertainties arise in the low temperature rate constants and in the isotopic branching ratio when reacting with HD.

* Dept. Química, Bioquímica e Farmácia, Universidade do Algarve, 8005-139 Faro, Portugal

Advances in Quantum Chemistry, Vol. 55
ISSN 0065-3276, DOI: 10.1016/S0065-3276(07)00203-1

1. INTRODUCTION

The absorption of radiation of wave lengths between 200 and 300 nm in the ozone stratospheric layer is a process of key importance in the reduction of ultra-violet radiation, which is known to cause biological mutations, solar burnings and other physiological effects [1]. The resultant oxygen atom in its lowest electronically excited state, O (^1D), see Eq. (1), is a highly reactive species that plays a significant role in initiating much stratospheric chemistry [2,3].

$$O_3 + h\nu\ (< 300\ \text{nm}) \rightarrow O\ (^1D) + O_2. \tag{1}$$

In particular, the excited oxygen atom quickly attacks methane, water vapor or molecular hydrogen present in stratosphere, see Figure 3.1, producing hydroxyl radicals according to reactions [4]

$$O\ (^1D) + H_2O \rightarrow OH + OH, \tag{2}$$

$$O\ (^1D) + CH_4 \rightarrow CH_3 + OH, \tag{3}$$

$$O\ (^1D) + H_2 \rightarrow H + OH. \tag{4}$$

These reactions constitute a source of OH in upper stratosphere, which ultimately controls the upper boundary of the ozone layer through the OH/HO_2 catalytic destruction cycles [5] getting rid of about 10% of the existing ozone [6]. The decrease of the ozone layer is a well known problem, see *e.g.* [3,7–9].

Due to its important role in atmospheric chemistry, the reaction

$$O\ (^1D) + H_2 \rightarrow H + OH, \qquad \Delta H_0^\circ = -181.4\ \text{kJ mol}^{-1}, \tag{5}$$

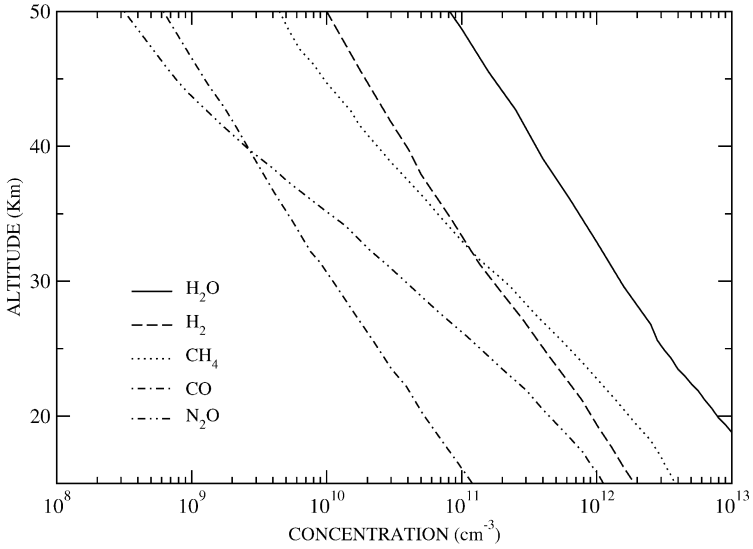

FIGURE 3.1 Gases present in stratosphere, adapted from reference [4].

and its isotopic variants

$$O(^1D) + D_2 \rightarrow D + OD, \qquad \Delta H_0^\circ = -179.7\ \text{kJ mol}^{-1}, \tag{6}$$

$$O(^1D) + HD \rightarrow D + OH, \qquad \Delta H_0^\circ = -177.9\ \text{kJ mol}^{-1}, \tag{7}$$

$$O(^1D) + HD \rightarrow H + OD, \qquad \Delta H_0^\circ = -183.8\ \text{kJ mol}^{-1}, \tag{8}$$

have been the subject of several experimental studies such as those observed in references [10–17]. Numerous theoretical studies of its dynamics have also been carried out, for example see [11,13,16–31], using several potential energy surfaces (PESs) published for this system [29,32–43]. These works have been the subject of partial reviews by Liu [44], Althorpe and Clary [45], Balucani *et al.* [46] and Aoiz *et al.* [47].

The title reaction is also of considerable interest to combustion [48] and laser chemistries [49]. Theoretically it is one of the best known complex-forming reactions from a fundamental point of view [50].

2. CHARACTERIZATION OF THE O (^1D) + H_2 REACTION

A general overview of the different potential energy surfaces relevant to the reactions involving an oxygen atom and the hydrogen molecule has been sketched in the work of Durand and Chapuisat [51].

As it can be seen in Figure 3.2, five potential energy surfaces are accessible to reactants but the mainly contribution comes from the lowest $\tilde{X}\,^1A'$ PES, which correlates with the $\tilde{X}\,^1A_1$ ground state of the H_2O molecule. In this PES the title reaction proceeds without energy barrier from reactants to products through a highly excited water molecule.

The first excited state, $\tilde{A}\,^1A''$, correlates with the ground state products OH ($X\,^2\Pi$) + H and must also be considered for energies higher than 8.4 kJ mol^{-1} [22], or temperatures above 500 K. The second excited state, $\tilde{B}\,^1A'$, adiabatically correlates with excited state products, OH ($A\,^2\Sigma^+$) + H. At collinear geometries these two surfaces correspond to a double degenerate Π state.

The other two upper PESs ($\tilde{B}\,^1A''$ and $\tilde{C}\,^1A'$ states) are repulsive and correspond to a double degenerate Δ state at collinear geometries and correlate with excited state products. Their contribution to the title reaction is negligible [22].

As it can be seen in Figure 3.2, at collinear geometries the ground $\tilde{X}\,^1A'$ state has Σ symmetry and adiabatically correlates with an excited $A\,^2\Sigma^+$ state of the hydroxyl radical. As a result there is a crossing between the Σ and Π states. Schatz and co-workers [12,22,23,52] estimated a constant contribution at collinear geometries from the $^1\Pi$ state of approximately 10%, due to the non adiabatic electrostatic coupling between the $^1\Sigma^+$ ($\tilde{X}\,^1A'$) and $^1\Pi$ ($\tilde{B}\,^1A'$ and $\tilde{A}\,^1A''$) states.

As a conclusion, in addition to the role of the lowest ($\tilde{X}\,^1A'$) PES the contribution of the two first excited states should be considered.

The reactions of ground state oxygen atom, O (^3P), with molecular hydrogen proceed in PESs with a high energy barrier, being the room-temperature rate con-

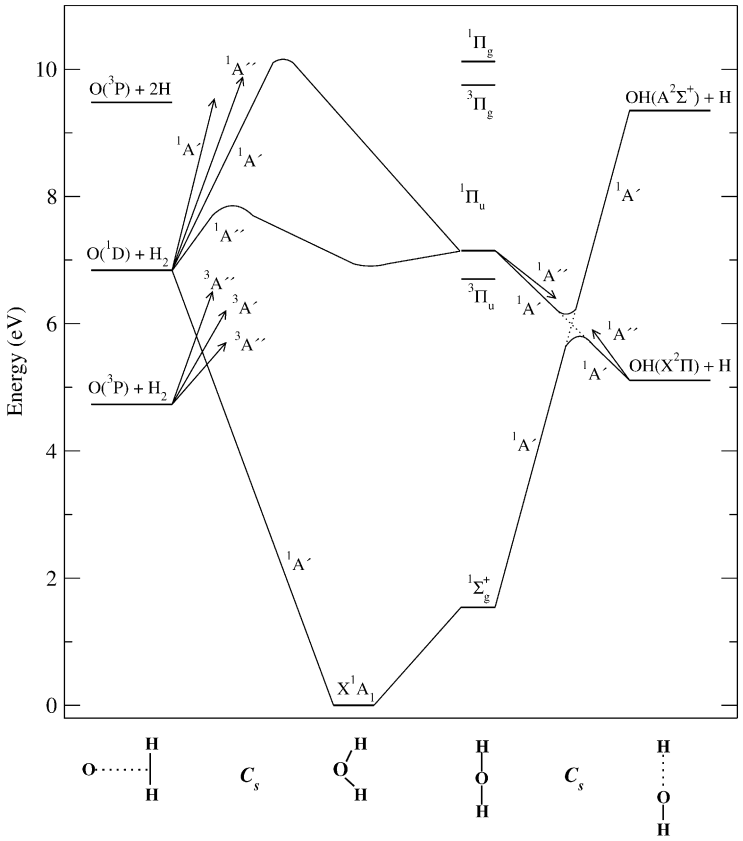

FIGURE 3.2 Correlation diagram of the potential energy surfaces involved in the O (^1D) + H_2 reaction, adapted from reference [51].

stant 10^{-7} times lower than that of O (^1D) + H_2 [53]. Most recently, Maiti and Schatz [54] and Chu *et al.* [55] have studied the intersystem crossing effects between the triplet and singlet states. Mainly focused on the O (^3P) + H_2 reaction, they found a negligible contribution to this reaction. In respect to the O (^1D) + H_2 reaction, Maiti and Schatz, using quasiclassical variant of the Trajectory Surface Hopping (TSH) approach [56], found that the intersystem cross effects on the O (^1D) + H_2 may decrease the adiabatic reactivity up to 10% through non reactive transitions to the triplet PESs. Chu *et al.* found a small reactivity on these PESs from a wave packet initiated on the $\tilde{X}\,^1A'$ PES. The net effect of the intersystem cross between triplet and singlet PESs is still an open question.

Although not shown in Figure 3.2, the H_2O ($\tilde{X}\,^1A'$) PES also correlates with the ground state triplet oxygen atom, O (^3P), and the triplet state hydrogen molecule, H_2 ($a\,^3\Sigma_u^+$). This is the lowest channel at large H–H distances [57] and should be also considered on a global PES for this system. Due to the very high energy of this region, the effects of this crossing on the dynamics of the title reaction should

be negligible. Nevertheless, this channel should be taken into account on a global PES.

3. POTENTIAL ENERGY SURFACES

To our knowledge, the first PES suitable for dynamical studies of the title reaction was proposed in 1976 by Murrell and Sorbie [58] from spectroscopic data, but the first dynamical studies have been carried out in 1980 by Schinke and Lester in a PES fitted from *ab initio* data [32]. To better reproduce the experimental rate constant, those authors propose two different potential energy surfaces named SL1 and SL3. Subsequently, Murrell, Carter, Mills and Guest have published a double-valued PES [57] to correctly account for the different crossings between the diabatic surfaces and Murrell and Carter proposed a simpler single-valued PES that approximates it [59]; this last one is known as MC PES.

The SL3 and MC PESs have shown to give quite different dynamical results for the O (^1D) + H_2 reaction. In a comparative study, Fitzgerald and Schatz [19] have shown that the MC PES favours a collinear approach of the O atom to the H_2 molecule, while the SL3 PES favours an insertion mechanism preceded by a perpendicular approach.

Kuntz *et al.* [60] using the diatomics-in-molecule (DIM) method constructed three slightly dfferent DIM PESs for the two lowest states. All these DIM PESs exhibit no barrier to reaction (insertion or abstraction) on the lowest surface.

Ten years ago Schatz and co-workers [61] proposed a new potential energy surface for the ground state $\tilde{X}\,^1A'$ H_2O PES fitted from *ab initio* MR-CI calculations using a triple zeta basis set and another for the first excited state $\tilde{A}\,^1A''$ H_2O PES [52]. Those PESs are known as K PESs. Lin and Guo [62] have observed that the $\tilde{X}\,^1A'$ H_2O K PES has an unphysical minimum of 50 cm^{-1} in the collinear H + OH asymptote, which caused convergence problems in calculating vibrational levels near the dissociation threshold [63].

One year later Dobbyn and Knowles presented three potential energy surfaces [64] that reproduce both $\tilde{X}\,^1A'$, $\tilde{A}\,^1A''$ and $\tilde{B}\,^1A'$ PESs and the non-adiabatic coupling between the $\tilde{X}\,^1A'$ and $\tilde{B}\,^1A'$ states [40]. Although extensively used in many calculations, as far as we know, there is not any publication describing in detail these DK PESs, only a brief presentation can be found in the work of Aoiz *et al.* [15].

In addition to the studies of the title reaction, the potential energy surface for the ground state water molecule is of great importance for roto-vibrational spectroscopic studies of this system. Therefore some PESs that accurately describe the bottom well have been published [35,37,65–67]. On the other hand those PES do not dissociate correctly and are not suitable for dynamical studies. In order to correct this behaviour, Varandas used an energy switching approach, joining the spectroscopic description of the bottom well with a semiempirical description of the van der Waals interactions between reactants or products, to build a global single-valued PES for the ground state water molecule [39], ES PES. This approach has been complemented with double and triple-valued potential energy surfaces (ES-2v and ES-3v PESs) for this system [41,42].

Recently, mainly based on the very accurate *ab initio* results of Partridge and Schwenke [66] complemented with other data [68,69] and on a careful description of the long range interactions between the different dissociation channels [70], Brandão and Rio presented another double-valued PES for this system [43]. This BR PES displays a small van der Waals minimum and a small saddle point under the dissociation limit for the C_{2v} approach of the O (^1D) atom to the H_2 molecule and a very small barrier ($< 0.4\,\mathrm{kJ\,mol^{-1}}$) to collinear addition ($^1\Sigma^+$ surface) in agreement with the findings of Walch and Harding [68].

4. DYNAMICAL STUDIES

The different potential energy surfaces have been used in several calculations of the dynamics of the title reaction using quasiclassical trajectory methods and quantum calculations, see references [71,72] for a general description of these methods. Some capture and statistical calculations have also been reported for this reaction.

4.1 Quantum calculations

Accurate quantum dynamical calculations for reactions with deep wells have been a major challenge to theoreticians. In this regard, due to the potential well depth of 7 eV corresponding to the stable water molecule, the reaction O (^1D) + H_2 → OH + H poses a formidable obstacle to exact quantum dynamical treatment. As a result, the earliest quantum calculation on this reaction was carried out by Badenhoop *et al.* [73] using a 2D model where the bending motion was treated by a sudden approximation.

With the increase of modern computer capacity and the development of quantum reactive scattering theories, such as the increasing implementation of Time Dependent Quantum Mechanical (TDQM) wave packet methods, full dimensional quantum calculations on the title reaction have been reported since 1996, first by Peng *et al.* [74] followed by Dai [75], by Balint-Kurti *et al.* [76] and by Gray *et al.* [77]. All these earlier quantum dynamical studies employed TDQM wave packet methods on the adiabatic ground electronic $\tilde{X}\,^1A'$ state having in mind the reaction mechanism (or the role of direct abstraction vs. insertion in the reaction mechanism). Among these works, Peng [74] and Dai [75] used the SL1 PES, while the works of Balint-Kurti [76] and Gray [77] were based on the K surface. Subsequent TDQM wave packet calculations [23,24,78–80] have been carried out mainly on the ground DK PES. The most recent wave packet calculations by Lin and Guo [62] used the BR PES to compute total cross sections and thermal rate constants.

Among those TDQM studies, exact quantum dynamical calculations were usually limited to the total angular momentum $J = 0$. For $J > 0$, most of the authors used a capture model (or L-shift model) [77] to estimate the reaction probability from the $J = 0$ results. Even the direct calculations of reaction probabilities for $J > 0$ were performed using the centrifugal sudden (CS) approximation. Carroll

and Goldfield [79] have reported wave packet calculations for $J > 0$ with inclusion of the Coriolis coupling terms. In comparison with the CS approximation results, these authors concluded that the CS approximation should yield accurate estimates of the reaction cross sections and rate constants for the title reaction.

The first exact quantum calculations of integral and differential cross sections on the adiabatic $\tilde{X}\,^1A'$ state were reported in 2001 by Honvault and Launay [15,81]. They have carried out quantum reactive scattering calculations of the title reaction on the DK PES within the Time Independent Quantum Mechanical (TIQM) framework using the hyperspherical close-coupling method.

The presence of five PESs correlating with the O (^1D) + H_2 reactants constitutes a further difficulty for the theoretical studies of the title reaction. Drukker and Schatz [22] have studied the effect of electronic Coriolis coupling in the entrance region for O (^1D) + H_2 using all five potential surfaces. In this work, the DK surfaces were used to describe the lowest three states while two DIM surfaces were employed for the upper two states. Using the vibrationally adiabatic coupled-channel approximation, they found that the upper two PESs ($\tilde{B}\,^1A''$ and $\tilde{C}\,^1A'$) are important only when considering the electronic fine structure of the reagents and the overall reactivity is dominated by the ground $\tilde{X}\,^1A'$ state with some influence of the first two excited $\tilde{A}\,^1A''$ and $\tilde{B}\,^1A'$ states. The participation of the $\tilde{A}\,^1A''$ and $\tilde{B}\,^1A'$ states in the title reaction has then been further investigated by a series of nonadiabatic quantum reactive scattering calculations using TDQM [23,24] or TIQM [26] as well as by some adiabatic TDQM or TIQM calculations on the $\tilde{A}\,^1A''$ surface [15,16,24,27,80,82].

Recently, Alexander *et al.* [29] carried out an *ab initio* study of the four states ($\tilde{X}\,^1A'$, $\tilde{A}\,^1A''$, $\tilde{a}\,^3A''$ and $\tilde{a}\,^3A'$) that correlate to OH–H in the product region and the electronic and spin-orbit couplings between them. These PESs were used to study the nonadiabatic effects on the branching between the product OH ($^2\Pi$) multiplet levels, using a statistical model of atom–diatom insertion reactions combined with coupled-states capture theory.

More recently and related to the title reaction and to the nonadiabatic effects, Chu *et al.* [55] reported an exact quantum wave-packet study of intersystem crossing effects for the O ($^3P_{2,1,0}$, $^1D_2$) + H_2 reaction, in which three triplets, $\tilde{a}\,^3A''$, $\tilde{b}\,^3A''$ and $\tilde{a}\,^3A'$, and one singlet, $\tilde{X}\,^1A'$, electronic states were employed.

4.2 Quasiclassical calculations

Almost all the published PESs have been used to perform quasiclassical trajectory (QCT) [71,83] studies of the title reaction. Those calculations have been mainly focused in adiabatic studies in each PES. In addition, the trajectory surface hopping method [56], has been used to study the nonadiabatic effects between the $\tilde{X}\,^1A'$ and $\tilde{B}\,^1A'$ PESs.

Excluding some details on the rotational energy distribution of the products, a general agreement has been found between the classical and quantum results when performed on the same PES. It's important to notice that the final attribution

of vibrational and rotational quantum levels obtained from quasiclassical calculations is a crude estimation. We also note that, due to the orbital and spin angular moments of the product OH $^2\Pi$ state, the classical angular moment of the OH diatomic, as computed in classical trajectories, differs from the nuclear rotational quantum number, N'.

At low temperatures, where quantum effects such as resonances can play an important role, the classical and quantum results for the thermal rate constant also diverge, as shown in Figure 3.11 of Section 5.5.

5. RESULTS AND COMPARISON WITH EXPERIMENT

Due to its importance, the reaction of O (^1D) + H_2 ($X\,^1\Sigma_g^+$) has been the subject of many experimental studies that can be compared with the theoretical predictions. For a recent review of the molecular beam experiments on the title reaction see the work of Balucani *et al.* [46].

5.1 Differential cross sections

The differential cross section is one of the most important results from molecular beam experiments. There we can see the differences between the insertion mech-

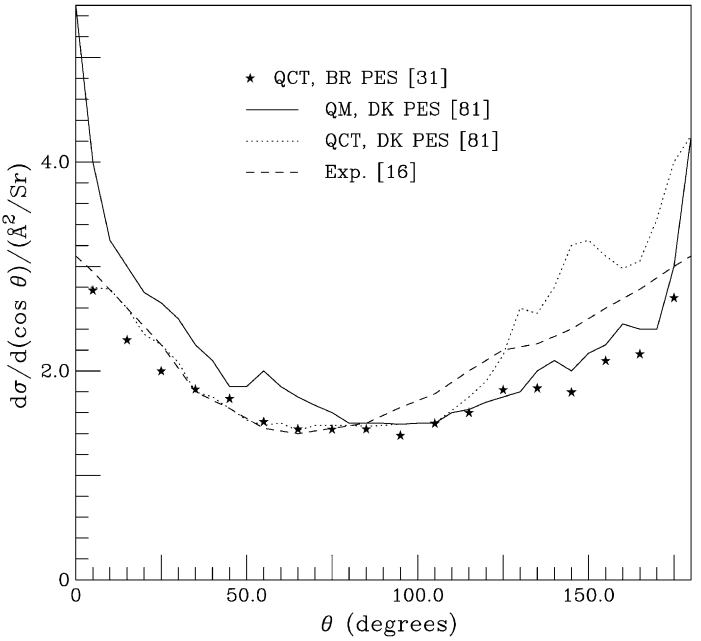

FIGURE 3.3 Angular distribution of the products for the reaction O (^1D) + H_2, at the collision energy of 5.4 kJ mol^{-1}.

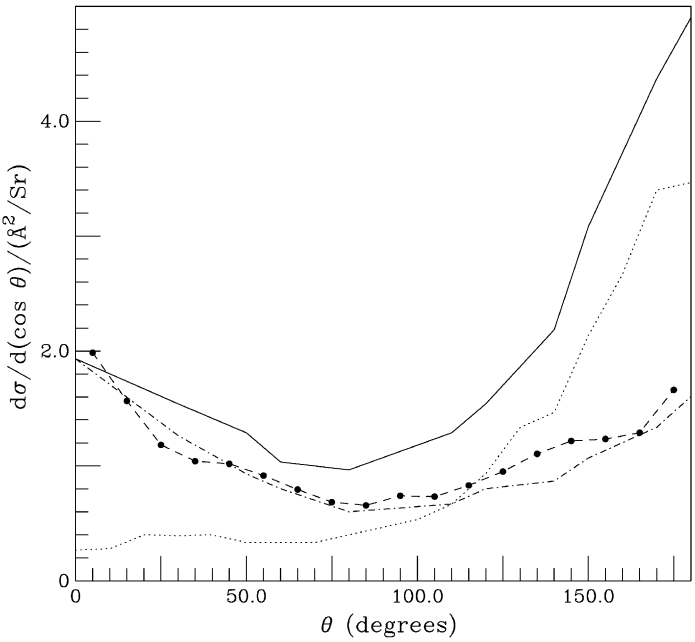

FIGURE 3.4 Angular distribution of the products for the reaction O (^1D) + HD → OD + H, at the collision energy of 19.0 kJ mol^{-1}. (—, · · · , - · - ·) represent the total, abstraction and insertion components obtained from the work of Hsu, Pederson and Schatz [12]. (- - -) displays the QCT results on the ground state BR PES [30].

anism of the reaction on the ground state PES that leads to forward-backward symmetry and the abstraction mechanism when the title reaction proceeds on the first excited state.

For this reason this property has been extensively computed using both quantum and classical methods, being the agreement between the experimental and the theoretical results using the most recent PESs generally good.

Figure 3.3 displays a comparison of the experimental differential cross section results at the collision energy of 5.4 kJ mol^{-1} with quantum and classical results on the $\tilde{X}\,^1A'$ DK and BR PESs. It is expected that only the ground state PES should contribute to reaction at this collision energy. Peculiarly, the DK PES gives a small anisotropy in opposite directions when comparing quantum and quasiclassical results. This discrepancy has been explained by Balucani *et al.* [17] as a result of quantum tunneling of the collisions with large angular moment through the centrifugal barrier, which is not accounted for in classical trajectory methods.

A different pattern is observed at 19.0 kJ mol^{-1} collision energy for the O + HD → OD + H reaction. At this higher energy we can see an additional contribution from the first excited state as plotted in Figure 3.4.

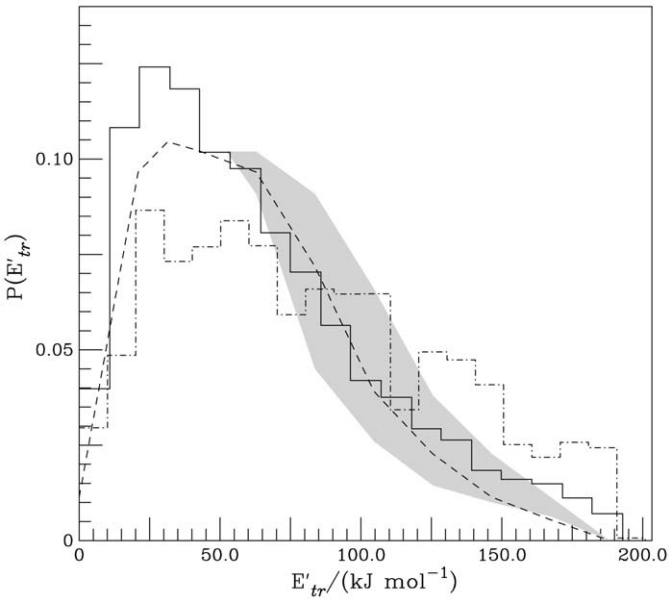

FIGURE 3.5 Translational energy distribution of the products of the reaction O (^1D) + H_2 at collision energy of 8.0 kJ mol^{-1} obtained by the QCT method (—) on BR PES and using statistical phase space calculations (- · - ·) [31]. The line (- - -) and the shaded area represent the experimental results and respective error bars [10].

5.2 Product energy distributions

The comparison between phase space [84] statistical calculations [31], experimental data and dynamical studies of the title reaction have shown that the dynamics of the OH_2 complex plays an important role on the energy distribution of the products. The higher rotational energy of the products has already been noted by Buss *et al.* [18] and has been explained as a result of the excitation of the vibrational bending mode due to the insertion mechanism. Despite the large exothermicity of this reaction, the long-range interactions have shown to play an important role on vibrational and rotational anisotropies of the OH product [85]. When using the DK PES and the coupled-channel statistical theory, Rackham *et al.* [86] have found a rotational distribution in close agreement with accurate quantum calculations on the same PES.

In Figure 3.5 we compare the experimental [10] translational energy distribution of the products of the reaction O (^1D) + H_2 at the collision energy of 8.0 kJ mol^{-1} with QCT results on the BR PES and statistical phase space results [31]. The agreement between the theoretical and experimental results seems reasonable.

The good agreement between theory and experiment is shown in Table 3.1 where we compare the experimental results of Aoiz *et al.* [14,15] at an average collision energy of 11.7 kJ mol^{-1} with QM and QCT calculations on the BR and DK PESs. In that work [14,15] the authors performed QCT and QM calculations

TABLE 3.1 Relation $P(\upsilon = 4)/P(\upsilon = 3)$

	BR PES QCT [31]	DK PES		Exp. [14,15]
		QCT [14,15]	QM [14,15]	
$\tilde{X}\,^1A'$ (only)	0.507	0.47 ± 0.01	0.53	–
$\tilde{X}\,^1A' + \tilde{A}\,^1A''$	–	0.60 ± 0.01	0.61	0.59 ± 0.05

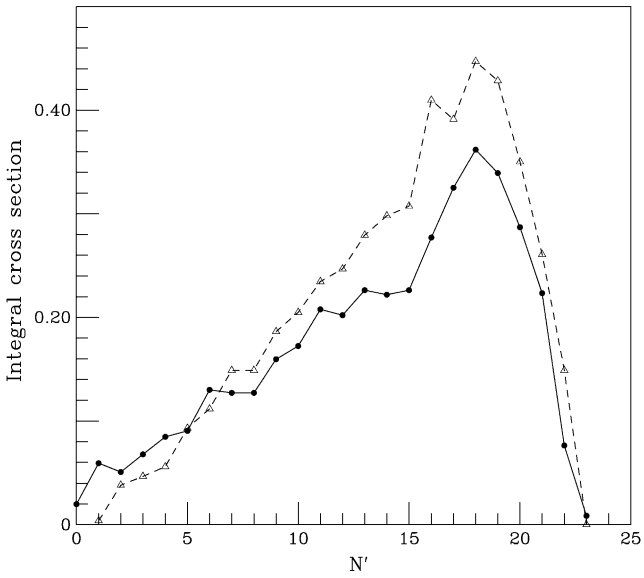

FIGURE 3.6 Experimental vs QCT rotationally integral cross section (in Å^2) for the O (^1D) + H_2 reaction, at 5.4 kJ mol^{-1} collision energy for $\upsilon' = 2$. Line (- - -, △), experimental data [16]; (—, ●) correspond to QCT results on BR PES [31].

both on the K and DK PESs and concluded that the DK surfaces present a better description for the dynamics of the reaction O (^1D) + H_2.

The inverted distribution of the rotational energy of the products is a characteristic property of this insertion reaction. Having in mind the above referred trouble in assigning the nuclear rotational quantum number, N', from classical trajectories (see Section 4.2), we show in Figure 3.6 a comparison between experimental [16] and QCT results on the BR PES [31] for the rotational integral cross section of the O (^1D) + H_2 reaction, at 5.4 kJ mol^{-1} collision energy for $\upsilon' = 2$. Here, the agreement is reasonably good.

5.3 Isotopic effects

The isotopic branching ratio, $\Gamma_{\mathrm{OD/OH}} = \sigma_r(\mathrm{OD{+}H})/\sigma_r(\mathrm{OH{+}D})$, of the products of the O (^1D) + HD reaction is the major divergence between theory and experiment

TABLE 3.2 Experimental isotopic branching ratio for O (^1D) + HD

E_{col} (kJ mol^{-1})	$\Gamma_{OD/OH}$	Ref.
2.1–6.7	1.03	[50]
8.6	1.17 ± 0.10	[50,88]
10.0	1.5 ± 0.2	[89]
10.0	1.3 ± 0.1	[89]
13.5	1.35 ± 0.20	[90]
14.2	1.4 ± 0.2	[89]
15.5	1.34	[50]
18.8	1.49	[50]
18.9	1.5	[91]
Room temp.	1.13 ± 0.08	[92]
$T = 298$ K	1.33 ± 0.07	[93]

TABLE 3.3 Reactive cross sections for O (^1D) + HD and isotopic branching ratio, $\Gamma_{OD/OH}$, using different PESs. All results but the last one refer to QCT calculations

E_{col} (kJ mol^{-1})	PES	$\sigma_{r(OH+D)}$ (Å^2)	$\sigma_{r(OD+H)}$ (Å^2)	$\Gamma_{OD/OH}$	Ref.
2.1	SL1	–	–	1.85 ± 0.24	[19]
	MC	–	–	1.08 ± 0.06	[19]
8.6	$^1A'$ DK	7.24	14.03	1.94	[87]
	$^1A'$ BR	6.19 ± 0.11	13.29 ± 0.12	2.15 ± 0.09	[30]
14.5[a]	$^1A'$ BR	5.50 ± 0.11	13.15 ± 0.16	2.38 ± 0.10	[30]
15.5	$^1A'$ BR	5.56 ± 0.10	11.76 ± 0.12	2.12 ± 0.10	[30]
19.0	$^1A'$ DK	6.28	11.46	1.82	[87]
	$^1A'$ K	6.94	10.59	1.53	[87]
	SL1	6.144	9.482	1.56 ± 0.02	[94]
	$^1A'$ BR	5.49 ± 0.10	11.27 ± 0.12	2.05 ± 0.10	[30]
20.9	SL1	–	–	1.4	[19]
	MC	–	–	1.09	[19]
Room temp.	WMF	–	–	4.5	[92]
	MCMG	–	–	2.0 ± 0.3	[95]
21.0–51.0	DK PESs	–	–	≈ 2	[26]

a Average value.

in this system. We collect in Table 3.2 the experimental data found in the literature for this branching ratio and, for comparison, we display in Table 3.3 the theoretical estimates using several potential energy surfaces for the lower adiabatic state. Comparing those tables we can see that the experimental value range is consistently lower than the theoretical ones, being these last results strongly dependent on the PES used in the calculations. From the most recent PESs, only the theoreti-

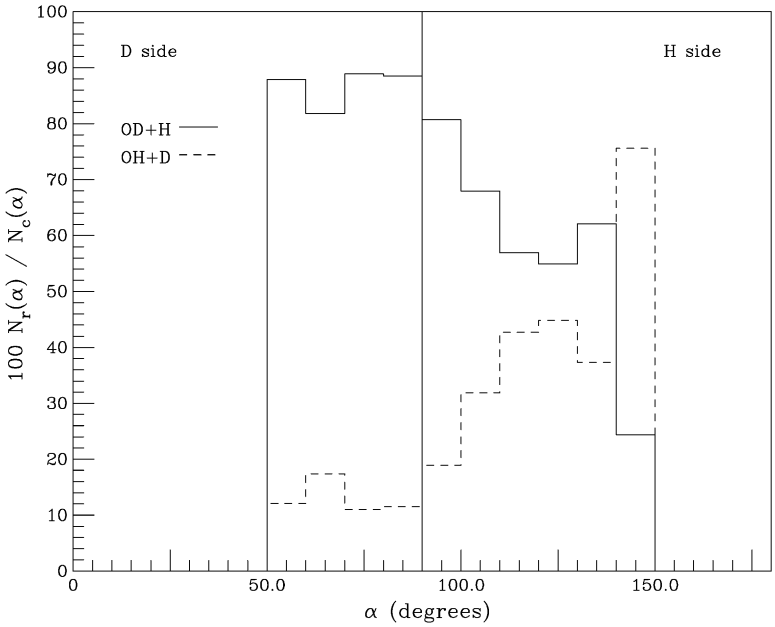

FIGURE 3.7 Reaction channel probability, in %, for each approach angle, α, for O (^1D) + HD at 2.05 kcal mol^{-1}.

cal results on the ground K PES agree with the higher experimental estimates. In addition, the role of the excited PES is expected to be small and contribute to a higher isotopic ratio [87].

To clarify the theoretical results, Fitzcharles and Schatz [19] discussed the angle of approach in the MC and SL1 PESs. They conclude that the MC PES favours a collinear collision where the first bond formed becomes the product diatomic, which explains an isotopic branching ratio close to one; on the other hand the SL1 PES leads to the formation of a tight complex, which dissociates into OD + H predominantly. Rio and Brandão [30] performed QCT results on the BR PES and found that, although the reaction proceeds through an insertion mechanism, those trajectories that reach the D atom side will dissociate in OD + H; but only those trajectories reaching the H side at a very high angle will dissociate as OH + D predominantly, as shown in Figure 3.7. In addition they found that during the complex lifetime there is an energy transfer process that favours the OD + H channel.

This divergence between theory and experiment is not so clear when we look at the distribution of the energy of the different dissociation channels. In Table 3.4 we compare the energy distribution of the products at the collision energies of 8.6 kJ mol^{-1} and 19.0 kJ mol^{-1}. We see a good agreement between the calculated and experimental results at the lower energy but at 19.0 kJ mol^{-1} the experimental results are too disperse to allow any conclusion. As far as we know, there is no experimental information on the partition of the internal energy of the diatomic.

TABLE 3.4 Distribution of translational, vibrational and rotational energy of the products of O (^1D) + HD

E_{col} (kJ mol^{-1})	Source	Channel	E_{tr} (%)	E_{vib} (%)	E_{rot} (%)	Ref.
8.6	BR PES	OD + H	32.44	41.50	26.06	[30]
		OH + D	26.50	37.53	35.97	[30]
	EXP.	OD + H	32	–	–	[11]
		OH + D	25	–	–	[11]
19.0	BR PES	OD + H	32.42	40.46	27.12	[30]
		OH + D	28.40	36.55	35.05	[30]
	SL1 PES	OD + H	33	40	28	[94]
		OH + D	28	39	32	[94]
	EXP.	OD + H	41 ± 9	–	–	[89]
		OH + D	19 ± 4	–	–	[89]
		OD + H	41 ± 7	–	–	[90]
		OH + D	32 ± 5	–	–	[90]
		OD + H	30	–	–	[91]
		OH + D	22	–	–	[91]

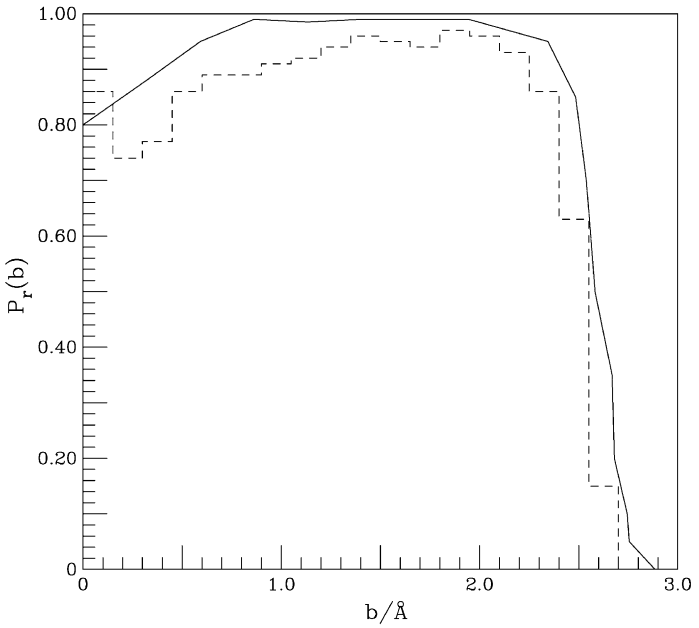

FIGURE 3.8 Opacity functions for the reaction O (^1D) + H_2 on the ground state PES. (—) corresponds to QM results on the DK PES at the collision energy of 9.6 kJ mol^{-1} [85] and (- - -) correspond to QCT results on BR PES at 8.0 kJ mol^{-1} collision energy [31].

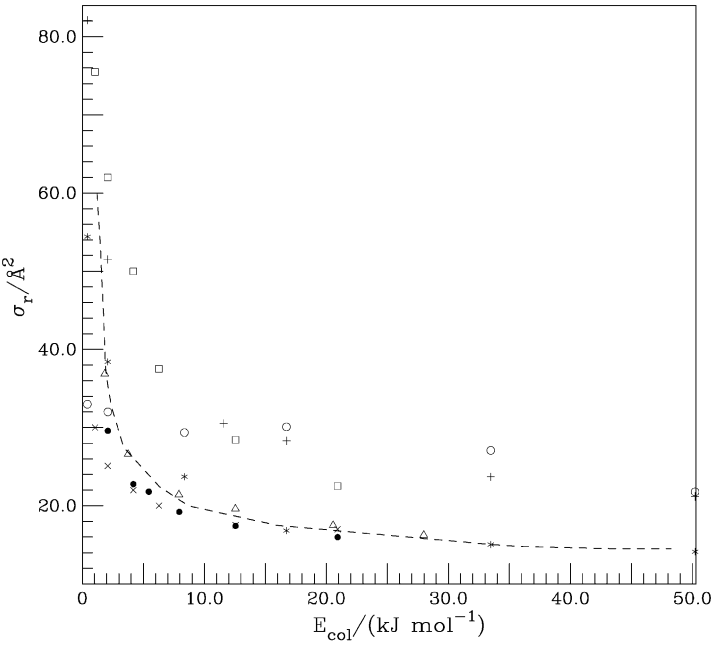

FIGURE 3.9 Comparison of QCT results of the total reactive cross section as a function of the collision energy for the reaction O (^1D) + H_2 using different published PESs. (●) BR PES [31]; (- - -) K PES [96]; (△) DK PES [24]; (+) ES PES [21]; (∗) ES-2v II PES [25]; (○) ES-2v III PES [25]; (×) SL1 PES [32] and (□) SL3 PES [32].

5.4 Total reactive cross sections

Due to limitations of the experiment, the molecular beam experiments are unable to measure the total cross section of the title reaction. As a consequence, here we can only compare the computed total cross sections using the different published PESs.

Closely related to the total cross section, the opacity function gives us the probability, $P_r(b)$, of a collision to be reactive at a given impact parameter, b. On the ground state PES, the title reaction proceeds without a barrier, being the reaction defined by the capture probability. As a consequence, the opacity function computed using the QCT method on the BR PES at different collision energies presents a similar form. As shown in Figure 3.8, the reaction probability is close to 0.9 for all collision energies at impact parameters less than 2.2 Å, vanishing quickly for larger impact parameters [31]. Rackham *et al.* [85] plotted the opacity function from accurate QM calculations [81] using the ground DK PES at the collision energy of 9.6 kJ mol^{-1}. These results, also plotted in Figure 3.8, display a similar trend with larger probability than on the BR PES at 8.0 kJ mol^{-1}, which is coherent with the larger reactivity found in the DK PES.

In Figure 3.9 we compare the QCT results for the total reactive cross section as a function of the collision energy computed by using different PESs. Varandas

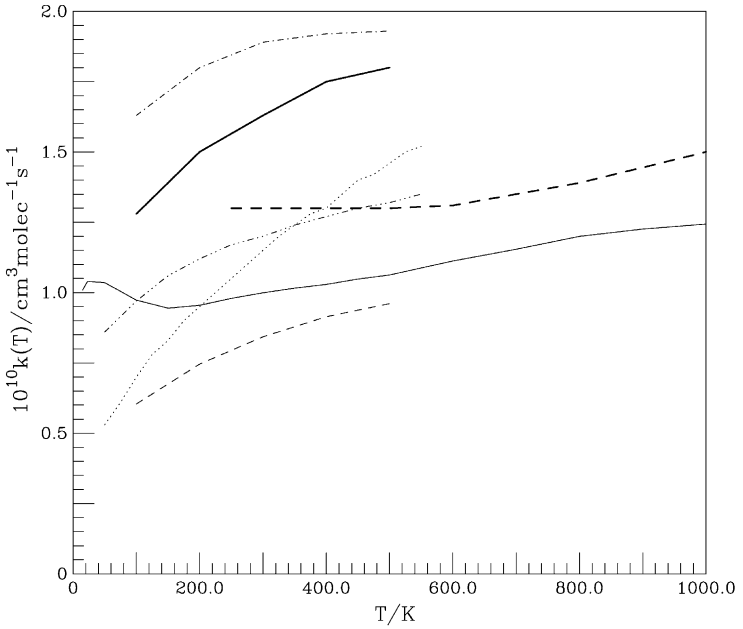

FIGURE 3.10 QCT thermal rate constants computed on the ground H_2O ($\tilde{X}\,^1A'$) PES. (—) BR PES [28]; (- - -) SL1 PES [32]; (- · - ·) SL3 PES [32]; (—) ES [21]; (- · · · · - · · · ·) ES-2v II [25]; (· · ·) ES-2v III [25] and (– – –) K PES [52].

et al. [25] have shown that the reactivity on the ES-2v PES strongly depends on the shape of the small bump for the C_{2v} insertion. Adding a Gaussian term, they have been able to propose two modifications of this PES, namely ES-2v II and ES-2v III, with different reactivities as shown in this figure.

We can see that the ES, ES-2v III and SL3 PES have a very different pattern with larger reactive total cross sections. The DK and K PESs have a very similar behaviour. Different is the ES-2v II PES which is similar to these PESs for energies above 17 kJ mol^{-1}, but has larger reactive cross section at 8 kJ mol^{-1} becoming smaller at very low collision energies. The BR and SL1 PESs are very similar being the BR more reactive at low collision energies.

These reactive total cross sections can be considered as the sum of a capture term, which decreases exponentially with energy, and a rigid sphere term, which is constant and should dominate at high collision energies [31].

$$\sigma(E) = \sigma_{\text{cap}}(E) + \sigma_{\text{rs}} = AE^{-m} + B. \tag{9}$$

The QM integral cross-section results of Lin and Guo [62] on the BR PES are not plotted in this figure. As shown in [31] these results are in good agreement with the QCT calculations in the same PES and somehow validates the use of classical mechanics in these studies.

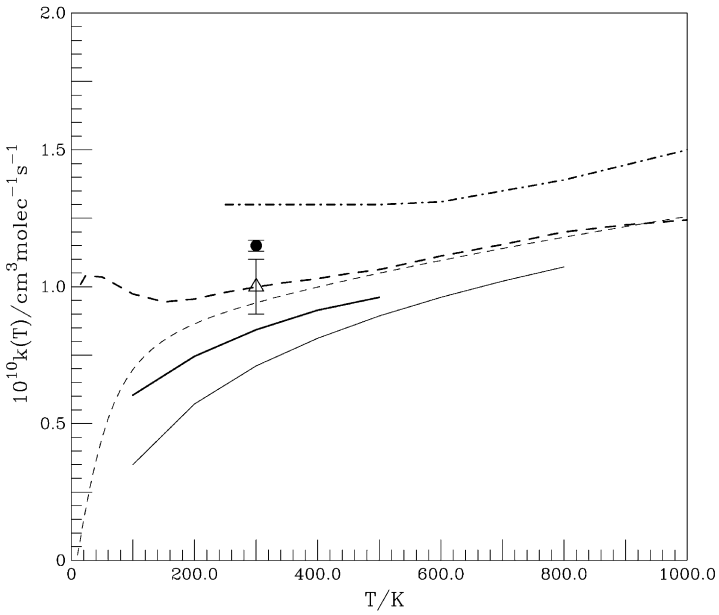

FIGURE 3.11 Comparison of QM and QCT thermal rate constants for the reaction O (^1D) + H_2, at different temperatures. (– – –) QCT [28] and (- - -) QM [62] results using the BR PES; (—) QCT [74] and (—) QM [74] results from the SL1 PES; line (- · - ·) QCT [52] and (●) QM results from the K PES [77] and (△) QM results on DK PES [77].

5.5 Thermal rate constants

A direct consequence of the different results for the total reactive cross section shown in Figure 3.9 is the diversity of the thermal rate constant computed using only the contribution of the ground H_2O ($\tilde{X}\,^1A'$) PES shown in Figure 3.10. In this figure we can see the higher reactivity of the SL3 and ES PESs and the high activation energy of the ES-2v III PES, which is a result of an almost constant reactive cross section. As expected the K and BR PESs display a parallel trend being the K PES more reactive. Also predictable from the low energy total cross sections is the behaviour of the SL1 PES, which has lower reactivity than the BR PES. The ES-2v II PES has lower reactivity at low temperatures but approaches (and even surpasses) the K PES as the temperature rises. So far as we know, there are not any published QCT results for the thermal constant computed using the DK PESs.

It is important to assess the role of quantum effects on the thermal rate constant. Unfortunately we only found QM thermal rate constant results for the SL1 [74] and BR PESs [62] at a large range of temperatures and two estimates for the K and DK PESs [77] at 300 K with a large uncertainty in the last one. In Figure 3.11 we compare these QM results with the correspondent QCT estimates. In all cases the QCT results lie above the QM predictions, being this difference larger in the SL1 PES. At temperatures above 400 K the QM and QCT results on the BR PES agree with each other, but at lower temperatures the differences become consid-

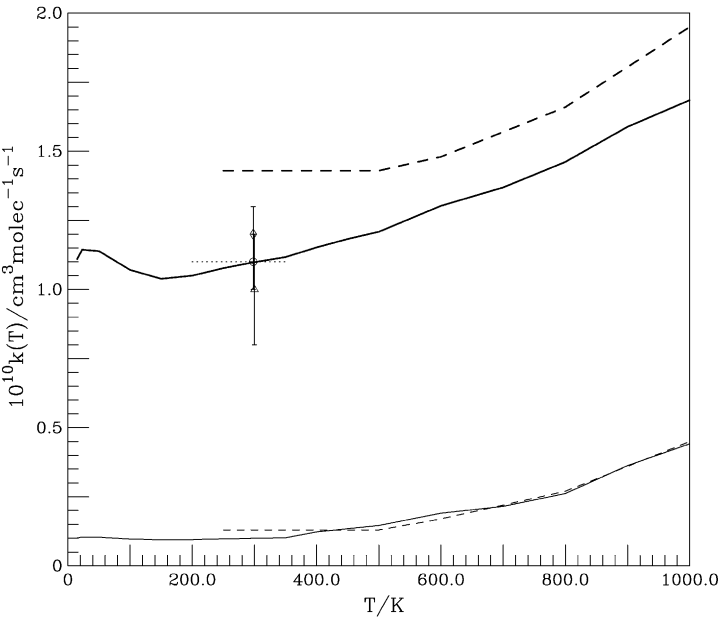

FIGURE 3.12 Thermal rate constants for the reaction O (^1D) + H_2, including the contribution from the excited PESs. (—) correction term and (—) estimated rate constant using the BR PES [28]. Line (- - -) correction term and (– – –) estimated rate constant using the K PES [52]. Most recent experimental data: (△) NASA report [3]; (· · ·) and (⊙) Atkinson [97] and (◇) Talukdar [93].

erable. Although some differences could reflect the restrictions of the quantum calculations, quantum effects should play an important role at low temperatures. This difference may be an indication of quantum effects due to resonances near the threshold. Another possible explanation is that, despite the agreement in the low energy cross sections, the QCT calculations are unable to account for the quantification of the angular moment, important at low energies. We also note that the QM results are not averaged over the possible internal states of the reactant diatomic.

As stated above when characterizing this reaction (see Section 2), two additional contributions should be taken into account before comparison with experiment. One is the abstraction reaction occurring in the first excited PES, H_2O ($\tilde{A}\,^1A''$), for temperatures higher than 500 K [22], being this contribution for the temperature of 1000 K approximately 0.3×10^{-10} cm^3 molec^{-1} s^{-1}. The other is the constant contribution from the $^1\Pi$ state of approximately 10% proposed by Schatz and co-workers [12,22,23,52], due to the non-adiabatic electrostatic coupling between the $^1\Sigma^+$ and $^1\Pi$ states at collinear geometries.

In Figure 3.12 we plot the estimated corrections from the upper PESs and a corrected estimate for the total thermal rate constant using both the BR PES [28] and K PES [52]. For comparison we also plot in this figure the experimental estimates for this thermal rate constant. There is a close agreement between the most recent experimental data and the QCT+corrections estimates of the thermal rate constant

from the BR PES. The higher reactivity found for the K PES is in accordance with the greater cross sections exhibit by this PES, as shown in Figure 3.9.

6. FINAL REMARKS AND CONCLUSIONS

We can conclude that there are accurate potential energy surfaces to describe the reaction O (^1D) + H_2, which plays an important role in the ozone depletion cycle. The most recent PESs correctly reproduce the molecular beam experimental results, namely, the differential cross sections and energy distribution of the products, including the contribution of the abstraction mechanism in the first excited PES, within the present experimental resolution.

In spite of these results, some subjects still need to be clarified. One is the isotopic branching ration in the reaction O (^1D) + HD, which shows a disagreement between the predictions of these PESs and the experimental results. This should be related with the details of the PES and the mechanism of energy transfer in the H_2O complex favouring one or other bond breaking. Another is the low temperature, below 200 K, thermal rate constant, where we found a clear divergence between classical and quantum results. This should clarify the role of long range van der Waals interactions in the dynamics of this reaction. A third still open question is the magnitude of the intersystem crossing effects between the singlet and triplet PESs on the title reaction.

We have entitled this work, "a well studied reaction", but the more we study this system the more questions need to be answered.

ACKNOWLEDGEMENTS

This work was supported by the FCT under the POCTI/CTA/41252/2001 Research Project, co-financed by the European Community Fund, FEDER.

REFERENCES

[1] T.E. Graedel, P.J. Crutzen, *Atmospheric Change—An Earth System Perspective*, W.H. Freeman and Company, New York, 1993.
[2] J.G. Anderson, *Ann. Rev. Phys. Chem.* **38** (1987) 489.
[3] S.P. Sander, *et al.*, Chemical Kinetics and Photochemical Data for Use in Atmospheric Studies, JPL Publication 06-2, NASA-Jet Propulsion Laboratory, Pasadena, California, 2006.
[4] M. Nicolet, *Adv. Chem. Phys.* **55** (1985) 63.
[5] S. Koppe, *et al.*, *Chem. Phys. Lett.* **214** (1993) 546.
[6] H.S. Johnston, *Annu. Rev. Phys. Chem.* **26** (1975) 315.
[7] J.W. Chamberlain, D.M. Hunten, *Theory of Planetary Atmospheres—An Introduction to Their Physics and Chemistry*, Academic Press, San Diego, 1987.
[8] J.R. Barker, A brief introduction to atmospheric chemistry, in: J.R. Barker (Ed.), *Progress and Problems in Atmospheric Chemistry*, World Scientific, Singapore, 1995, pp. 1–33.
[9] J.H. Seinfeld, Chemistry of ozone in the urban and regional atmosphere, in: J.R. Barker (Ed.), *Progress and Problems in Atmospheric Chemistry*, World Scientific, Singapore, 1995, pp. 34–57.
[10] M. Alagia, *et al.*, *J. Chem. Phys.* **108** (1998) 6698.

[11] Y.-T. Hsu, K. Liu, L.A. Pederson, G.C. Schatz, *J. Chem. Phys.* **111** (1999) 7921.
[12] Y.-T. Hsu, K. Liu, L.A. Pederson, G.C. Schatz, *J. Chem. Phys.* **111** (1999) 7931.
[13] M. Ahmed, D.S. Peterka, A.G. Suits, *Chem. Phys. Lett.* **301** (1999) 372.
[14] F.J. Aoiz, *et al.*, *Dynamics of the O* $(^1D) + H_2 \rightarrow OH\ (v = 3, 4; N) + H$, book of 13th European Conference on Dynamics of Molecular Collisions (MOLEC 2000), A.26, Jerusalém, Israel, 17–22 September, 2000, p. 78.
[15] F.J. Aoiz, *et al.*, *Phys. Rev. Lett.* **86** (2001) 1729.
[16] F.J. Aoiz, *et al.*, *J. Chem. Phys.* **116** (2002) 10692.
[17] N. Balucani, *et al.*, *Mol. Phys.* **103** (2005) 1703.
[18] R.J. Buss, P. Casavecchia, S.J. Sibener, Y.T. Lee, *Chem. Phys. Lett.* **82** (1981) 386.
[19] M.S. Fitzcharles, G.C. Schatz, *J. Phys. Chem.* **90** (1986) 3634.
[20] T.-S. Ho, T. Hollebeek, H. Rabitz, L.B. Harding, G.C. Schatz, *J. Chem. Phys.* **105** (1996) 10472.
[21] A.J.C. Varandas, A.I. Voronin, A. Riganelli, P.J.S.B. Caridade, *Chem. Phys. Lett.* **278** (1997) 325.
[22] K. Drukker, G.C. Schatz, *J. Chem. Phys.* **111** (1999) 2451.
[23] S. Gray, C. Petrongolo, K. Drukker, G. Schatz, *J. Phys. Chem. A* **103** (1999) 9448.
[24] S.K. Gray, *et al.*, *J. Chem. Phys.* **113** (2000) 7330.
[25] A.J.C. Varandas, A.I. Voronin, P.J.S.B. Caridade, A. Riganelli, *Chem. Phys. Lett.* **331** (2000) 331.
[26] T. Takayanagi, *J. Chem. Phys.* **116** (2002) 2439.
[27] F.J. Aoiz, L. Banares, J.F. Castillo, V.J. Herrero, B. Martinez-Haya, *Phys. Chem. Chem. Phys.* **4** (2002) 4379.
[28] J. Brandão, C.M.A. Rio, *Chem. Phys. Lett.* **377** (2003) 523.
[29] M.H. Alexander, E.J. Rackham, D.E. Manolopoulos, *J. Chem. Phys.* **121** (2004) 5221.
[30] C. Rio, J. Brandão, *Chem. Phys. Lett.* **433** (2007) 268.
[31] C. Rio, J. Brandão, *Mol. Phys.* **105** (2007) 359.
[32] R. Schinke, W.A. Lester Jr., *J. Chem. Phys.* **72** (1980) 3754.
[33] J.N. Murrell, S. Carter, S.C. Farantos, P. Huxley, A.J.C. Varandas, *Molecular Potential Energy Functions*, Wiley, Chichester, 1984.
[34] L. Halonen, T. Carrington, *J. Chem. Phys.* **88** (1988) 4171.
[35] P. Jensen, *J. Mol. Spectrosc.* **133** (1989) 438.
[36] E. Kauppi, L. Halonen, *J. Phys. Chem.* **94** (1990) 5779.
[37] O. Polyansky, P. Jensen, J. Tennyson, *J. Chem. Phys.* **101** (1994) 7651.
[38] A.J.C. Varandas, A.I. Voronin, *Mol. Phys.* **85** (1995) 497.
[39] A.J.C. Varandas, *J. Chem. Phys.* **105** (1996) 3524.
[40] A.J. Dobbyn, P.J. Knowles, *Mol. Phys.* **91** (1997) 1107.
[41] A.J.C. Varandas, *J. Chem. Phys.* **107** (1997) 867.
[42] A.J.C. Varandas, A.I. Voronin, P.J.S.B. Caridade, *J. Chem. Phys.* **108** (1998) 7623.
[43] J. Brandão, C.M.A. Rio, *J. Chem. Phys.* **119** (2003) 3148.
[44] K. Liu, *Annu. Rev. Phys. Chem.* **52** (2001) 139.
[45] S.C. Althorpe, D.C. Clary, *Annu. Rev. Phys. Chem.* **54** (2003) 493.
[46] N. Balucani, G. Capozza, F. Leonori, E. Segoloni, P. Casavecchia, *Int. Rev. Phys. Chem.* **25** (2006) 109.
[47] F. Aoiz, L. Banares, V. Herrero, *J. Phys. Chem. A* **110** (2006) 12546.
[48] G. Dixon-Lewis, D.J. Williams, The oxidation of hydrogen and carbon monoxide, in: C.H. Bamford, C.F.H. Tipper (Eds.), in: *Comprehensive Chemical Kinetics*, vol. 17, Elsevier, Amsterdam, 1977, pp. 1–248.
[49] A.B. Callear, H.E. Van den Bergh, *Chem. Phys. Lett.* **8** (1971) 17.
[50] Y.-T. Hsu, J.-H. Wang, K. Liu, *J. Chem. Phys.* **107** (1997) 2351.
[51] G. Durand, X. Chapuisat, *Chem. Phys.* **96** (1985) 381.
[52] G.C. Schatz, *et al.*, *J. Chem. Phys.* **107** (1997) 2340.
[53] R.N. Dubinsky, D.J. McKenney, *Can. J. Chem.* **53** (1975) 3531.
[54] B. Maiti, G.C. Schatz, *J. Chem. Phys.* **119** (2003) 12360.
[55] T.-S. Chu, X. Zhang, K.-L. Han, *J. Chem. Phys.* **122** (2005) 214301.
[56] J.C. Tully, *J. Chem. Phys.* **93** (1990) 1061.
[57] J.N. Murrell, S. Carter, I.M. Mills, M.F. Guest, *Mol. Phys.* **42** (1981) 605.
[58] K.S. Sorbie, J.N. Murrell, *Mol. Phys.* **29** (1975) 1387.
[59] J.N. Murrell, S. Carter, *J. Phys. Chem.* **88** (1984) 4887.

[60] P.J. Kuntz, B.I. Niefer, J.J. Sloan, *J. Chem. Phys.* **88** (1988) 3629.
[61] G.C. Schatz, *et al.*, *J. Chem. Phys.* **105** (1996) 10472.
[62] S.Y. Lin, H. Guo, *Chem. Phys. Lett.* **385** (2004) 193.
[63] S. Gray, E. Goldfield, *J. Phys. Chem. A* **105** (2001) 2634.
[64] A.J. Dobbyn, P.J. Knowles, *Faraday Discuss.* **110** (1998) 247.
[65] P. Jensen, S.A. Tashkun, V.G. Tyuterev, *J. Mol. Spectrosc.* **168** (1994) 271.
[66] H. Partridge, D.W. Schwenke, *J. Chem. Phys.* **106** (1997) 4618.
[67] O.L. Polyansky, P. Jensen, J. Tennyson, *J. Chem. Phys.* **105** (1996) 6490.
[68] S.P. Walch, L.B. Harding, *J. Chem. Phys.* **88** (1988) 7653.
[69] F. Schneider, F.D. Giacomo, F.A. Gianturco, *J. Chem. Phys.* **104** (1996) 5153.
[70] J. Brandão, C.M.A. Rio, *Chem. Phys. Lett.* **372** (2003) 866.
[71] D.G. Truhlar, J.T. Muckerman, Reactive scattering cross sections iii. Quasiclassical and semiclassical methods, in: R.B. Bernstein (Ed.), *Atom—Molecule Collision Theory*, Plenum Press, New York, 1979, pp. 505–566.
[72] J.Z.H. Zhang, *Theory and Application of Quantum Molecular Dynamics*, World Scientific, Singapore, 1999.
[73] K. Badenhoop, H. Koizumi, G.C. Schatz, *J. Chem. Phys.* **91** (1989) 142.
[74] T. Peng, D.H. Zhang, J.Z.H. Zhang, R. Schinke, *Chem. Phys. Lett.* **248** (1996) 37.
[75] J. Dai, *J. Chem. Phys.* **107** (1997) 4934.
[76] G.G. Balint-Kurti, A.I. Gonzalez, E.M. Goldfield, S.K. Gray, *Faraday Discuss.* **110** (1998) 169.
[77] S.K. Gray, E.M. Goldfield, G.C. Schatz, G.G. Balint-Kurti, *Phys. Chem. Chem. Phys.* **1** (1999) 1141.
[78] M. Hankel, G.G. Balint-Kurti, S.K. Gray, *J. Chem. Phys.* **113** (2000) 9658.
[79] T. Carroll, E. Goldfield, *J. Phys. Chem. A* **105** (2001) 2251.
[80] M. Hankel, G. Balint-Kurti, S. Gray, *J. Phys. Chem. A* **105** (2001) 2330.
[81] P. Honvault, J.-M. Launay, *J. Chem. Phys.* **114** (2001) 1057.
[82] F.J. Aoiz, L. Banares, J.F. Castillo, B. Martinez-Haya, M.P. de Miranda, *J. Chem. Phys.* **114** (2001) 8328.
[83] J.T. Muckerman, *J. Chem. Phys.* **54** (1971) 1155.
[84] P. Pechukas, J.C. Light, C. Rankin, *J. Chem. Phys.* **44** (1966) 794.
[85] E.J. Rackham, T. Gonzalez-Lezana, D.E. Manolopoulos, *J. Chem. Phys.* **119** (2003) 12895.
[86] E.J. Rackham, F. Huarte-Larranaga, D.E. Manolopoulos, *Chem. Phys. Lett.* **343** (2001) 356.
[87] F.J. Aoiz, L. Bañares, M. Brouard, J.F. Castillo, V.J. Herrero, *J. Chem. Phys.* **113** (2000) 5339.
[88] S.-H. Lee, K. Liu, *Chem. Phys. Lett.* **290** (1998) 323.
[89] Y. Matsumi, K. Tonokura, M. Kawasaki, H.L. Kim, *J. Phys. Chem.* **96** (1992) 10622.
[90] T. Laurent, *et al.*, *Chem. Phys. Lett.* **236** (1995) 343.
[91] D.C. Che, K. Liu, *J. Chem. Phys.* **103** (1995) 5164.
[92] K. Tsukiyama, B. Katz, R. Bersohn, *J. Chem. Phys.* **83** (1985) 2889.
[93] R.K. Talukdar, A.R. Ravishankara, *Chem. Phys. Lett.* **253** (1996) 177.
[94] A.J. Alexender, F.J. Aoiz, M. Brouard, J.P. Simons, *Chem. Phys. Lett.* **256** (1996) 561.
[95] L.J. Dunne, *Chem. Phys. Lett.* **158** (1989) 535.
[96] A.J. Alexander, *et al.*, *Chem. Phys. Lett.* **278** (1997) 313.
[97] R. Altkinson, *et al.*, *J. Phys. Chem. Ref. Data* **21** (1992) 1125.